Title

Tunable Polaron Distortions Control the Extent of Halide Demixing in Lead Halide Perovskites

Journal

The Journal of Physical Chemistry Letters, 9(14)

ISSN

1948-7185

Authors

Bischak, Connor G

Wong, Andrew B

Lin, Elbert

et al.

Publication Date

2018-07-19

DOI

10.1021/acs.jpclett.8b01512

Peer reviewed

THE JOURNAL OF PHYSICAL CHEMISTRY Letters

Cite This: J. Phys. Chem. Lett. 2018, 9, 3998−4005

Letter

pubs.acs.org/JPCL

Tunable Polaron Distortions Control the Extent of Halide Demixing in Lead Halide Perovskites

Connor G. Bischak,[†,∇,¶] Andrew B. Wong,[†,○,¶] Elbert Lin,[†,◆] David T. Limmer,[†,‡,§] Peidong Yang,[†,‡,§,∥] and Naomi S. Ginsberg*[,†,‡,§,⊥,#]

[†]Department of Chemistry, University of California, Berkeley, California 94720, United States

[‡]Kavli Energy NanoScience Institute, Berkeley, California 94720, United States

[§]Materials Science Division, Lawrence Berkeley National Laboratory, Berkeley, California 94720, United States

[∥]Department of Materials Science and Engineering, University of California, Berkeley, California 94720, United States

[⊥]Molecular Biophysics and Integrated Bioimaging Division, Lawrence Berkeley National Laboratory, Berkeley, California 94720, United States

[#]Department of Physics, University of California, Berkeley, California 94720, United States

Supporting Information

ABSTRACT: Photoinduced phase separation in mixed halide perovskites emerges from their electro-mechanical properties and high ionic conductivities, resulting in photoinduced I^--rich charge carrier traps that diminish photovoltaic performance. Whether photoinduced phase separation stems from the polycrystalline microstructure or is an intrinsic material property has been an open question. We investigate the nanoscale photoinduced behavior of single-crystal mixed Br^-/I^- methylammonium (MA^+) lead halide perovskite ($MAPb(Br_xI_{1-x})_3$) nanoplates, eliminating effects from extended structural defects. Even in these nanoplates, we find that phase separation occurs, resulting in I^--rich clusters that are nucleated stochastically and stabilized by polarons. Upon lowering the electron−phonon coupling strength by partially exchanging MA^+ for Cs^+, a phase-separated steady state is not reached, nevertheless transient I^- clustering still occurs. Our results, supported by multiscale modeling, demonstrate that photoinduced phase separation is an intrinsic property of mixed halide perovskites, the extent and dynamics of which depends on the electron−phonon coupling strength.

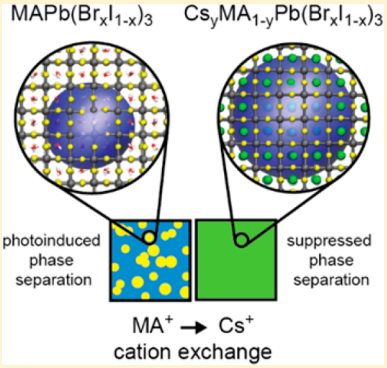

The dynamic behavior of lead halide perovskites stems from a novel combination of electronic and mechanical material properties, which together lead to unintended phenomena that impact halide perovskite-based devices. Halide perovskites have the chemical formula ABX_3, where A is either an organic cation such as methylammonium (MA^+) or Cs^+, B is typically Pb^{2+}, and X is a halide or halide mixture (Br^-/Cl^- or I^-/Br^-). These materials undergo many dynamic processes across a wide range of length and time scales, including rotational motions of organic cations,[1,2] halide migration,[3,4] and long charge carrier lifetimes,[5−7] which influence lead halide perovskite device performance. Mixed halide perovskites have been intensely investigated for applications in optoelectronic devices such as light-emitting diodes (LEDs),[8,9] nanoscale lasers,[10,11] and tandem solar cells[12−14] because their bandgap can be easily and continuously tuned by varying the ratio of halides (Br^- to Cl^- or I^- to Br^-).[15−17] Unfortunately, under illumination, the halides in mixed halide perovskites reversibly phase separate, forming photoinduced charge-carrier traps that limit the utility of mixed halide perovskites for devices.[3,18−31]

Many investigations into photoinduced phase separation have been performed on mixed halide perovskite polycrystalline thin films,[3,18−26] which have a complex microstructure that depends greatly on the preparation method used. In polycrystalline films, it has therefore been difficult to determine to what extent photoinduced phase separation is facilitated or influenced by the presence of defects−especially grain boundaries, at which low-bandgap halide enrichment has been observed. Other studies have also explored photoinduced phase separation in polycrystalline thin films using different A-site cations with mixed results. For instance, polycrystalline thin films of mixed halide perovskites with a mixture of formamidinium (FA^+) and Cs^+ in the A site have shown no photoinduced phase separation in both the low and high illumination intensity limits,[13] whereas demixing was observed in mixed FA^+/Cs^+ thin films in a different study[31] and in polycrystalline thin films of entirely Cs-based mixed halide perovskites.[19] In these studies, it is challenging to decouple the

Received: May 13, 2018
Accepted: July 2, 2018
Published: July 6, 2018

DOI: 10.1021/acs.jpclett.8b01512
J. Phys. Chem. Lett. 2018, 9, 3998−4005

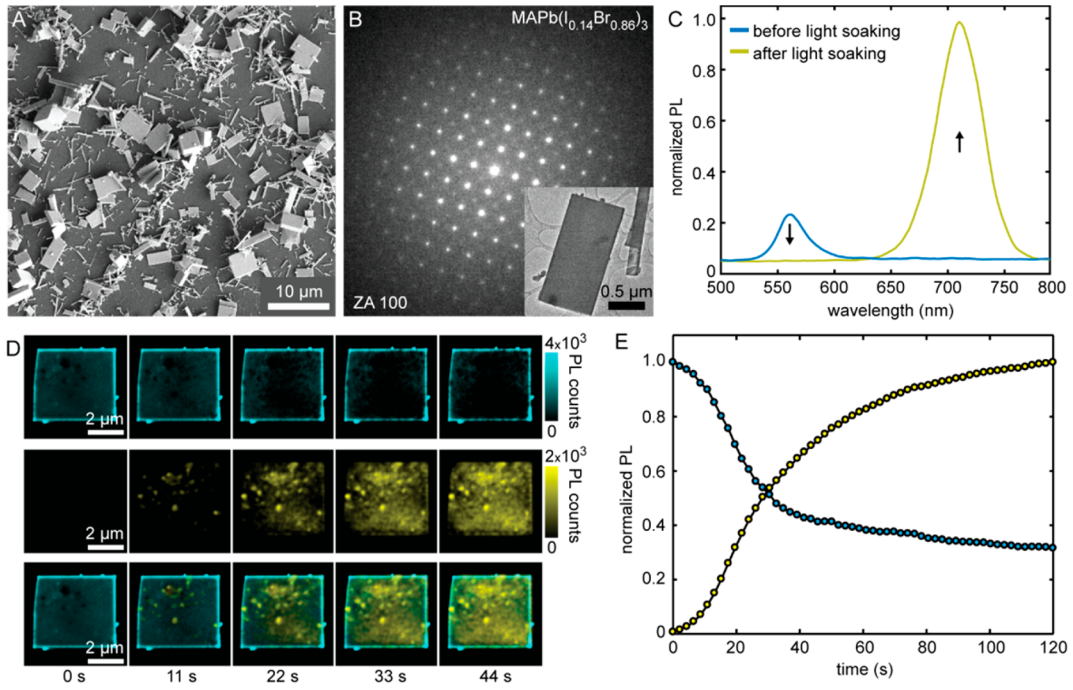

Figure 1. Photoinduced phase separation in mixed halide hybrid perovskite single-crystalline plates. (A) Scanning electron microscopy (SEM) image of nanowires and nanoplates as synthesized. (B) Low-dose transmission electron microscopy (TEM) selected area electron diffraction (SAED) pattern of a single-crystalline nanoplate aligned to the 100 zone axis (ZA). The inset shows a TEM image of the nanoplate, on which SAED was performed. (C) Photoluminescence (PL) emission spectra of a single nanoplate before and after illumination, showing the emergence of a red-shifted peak that corresponds to iodide-rich regions in the plate. (D) A series of confocal microscopy images with emission at 500−560 nm (cyan), 650−750 nm (yellow), and overlay of both channels excited at 405 nm at 12 μW with an 8 μs pixel dwell time (75 mJ/cm^2). (E) Trace of the photoluminescence intensity over the entire plate as a function of time.

effect of using different A site cations with associated variations in thin film morphology and defect structure. Additionally, Barker et al. hypothesize that charge carrier generation gradients through the thickness of the mixed halide film drive halide phase separation.[22] They indicate that this phenomenon would result in an enrichment of I^- at the surface of the film. Yet, Cappel et al. observe Br^- enrichment at the surface upon illumination,[32] so it has remained inconclusive which halide becomes more abundant at the surface upon light exposure.

We previously used cathodoluminescence (CL) imaging and multiscale modeling to determine that photoinduced phase separation is a nonequilibrium phenomenon driven by the presence of polarons—photogenerated charge carriers and their accompanying lattice distortions.[21] CL imaging enables high-resolution spatial mapping of the emission of lead halide perovskites.[33−38] Due to strong electron−phonon coupling in hybrid halide perovskites,[39−45] polaronic strain locally changes the free energy of halide mixing, leading to stabilized regions enriched in I^-. We showed that I^--rich clusters are stabilized by the presence of a photogenerated trapped polaron and that these clusters form stochastically upon illumination due to fluctuation in the local I^- concentration resulting from high halide mobility. Additionally, by replacing a more polarizable cation, such as MA^+, with a less polarizable cation, such as Cs^+, we demonstrated a significant decrease in the rate and extent of photoinduced phase separation. The film morphology, however, differed dramatically between perovskite thin films formed with MA^+- and Cs^+-containing precursors. Although the combination of CL imaging and multiscale modeling revealed the connection between halide phase separation and polaronic strain, how the halide perovskite morphology and presence of intrinsic structural defects, such as grain boundaries, affects photoinduced phase separation has remained poorly understood.

By investigating photoinduced phase separation in single-crystalline mixed halide hybrid perovskites nanoplates, we demonstrate that photoinduced phase separation is an intrinsic property of the material. That is, the demixing is not caused by specific features in the underlying microstructure and is instead related to intrinsic properties such as strong electron−phonon coupling, halide mixture-dependent band gaps, and halide diffusion. By using single crystals plates (~200 nm thick), we emulate the large grains found in high efficiency perovskite photovoltaics. Using a combination of CL and confocal microscopies, we observe the process of photoinduced phase separation in crystalline mixed halide perovskites, and we employ molecular modeling to confirm that polaronic strain, rather than I^- enrichment at grain boundaries, drives photoinduced phase separation. We show that stable I^--rich clusters form in the middle of single-crystalline perovskite nanoplates, not only at the edges, and that clusters emerge in different locations each time the reversible processes is performed. To evaluate the extent to which electron−phonon coupling strength affects photoinduced I^--rich cluster stability, we also developed a cation exchange method to postsynthetically replace the highly polarizable MA^+ cations with less polarizable Cs^+ cations. The cation exchange maintains the morphology of the nanoplates, thereby decoupling the effects of morphology and composition on photoinduced phase separation. In the mixed MA^+/Cs^+ mixed halide perovskites, although transient I^- clustering is still observed, the I^--rich

DOI: 10.1021/acs.jpclett.8b01512
J. Phys. Chem. Lett. 2018, 9, 3998−4005

clusters are not stabilized upon sustained illumination. Theoretical analysis suggests that the reduction in lattice polarizability results in a weaker interaction between free charges and the ionic lattice. Therefore, a phase-separated steady state is not reached because the electron−phonon coupling is insufficiently strong for polaronic strain to locally favor halide demixing. Our observations demonstrate that photoinduced phase separation occurs stochastically and results from intrinsic properties of the bulk perovskite material. Even when steady state phase separation is prevented due to compositional engineering of electron−phonon coupling, transient charge carrier traps are still present.

We first synthesize single-crystalline mixed halide perovskite nanoplates with the chemical formula $MAPb(I_{0.14}Br_{0.86})_3$ and demonstrate that photoinduced phase separation occurs in these materials despite the absence of grain boundaries. Nanoplates and nanowires were synthesized using the direct reaction of lead acetate with a mixture of methylammonium iodide and methylammonium bromide dissolved in 2-propanol (Figure 1A).[9,10] Low-dose selected area electron diffraction (SAED) confirms that the resulting nanoplates are single-crystalline (Figure 1B), and scanning transmission electron microscopy (STEM) energy dispersive X-ray spectroscopy (EDS) demonstrates that the halide ratio is 14:86 I^- to Br^- (Figure S1). Upon above-bandgap illumination of the perovskite nanoplates at 405 nm, we observe the emergence of a red-shifted peak, corresponding to the formation of I^--rich clusters (Figure 1C). In this study, we use both low electron exposure CL and confocal microscopies to interrogate photoinduced phase separation. CL microscopy has the advantage of subdiffraction limit spatial resolution and the ability to correlate luminescence spatially with morphology. The number of frames is, however, limited because of potential electron beam damage. As a complementary technique, confocal imaging allows for high frame rates and long acquisition times, and it avoids potential electron beam-induced damage. To show that photoinduced phase separation occurs in the synthesized single-crystalline nanoplates, we capture the emergence of I^--rich clusters in two separate emission channels, corresponding to the original emission wavelength range (500−560 nm) and the emission wavelength range of the emerging I^--rich clusters (650−750 nm), using confocal microscopy (Figure 1D). By overlaying the images from these two channels, we observe that they are anticorrelated (Figure 1D). We note that the edges of the nanoplates show enhanced PL, which likely stems from either photonic waveguiding effects[46] or a lower concentration of MA^+ vacancies at the edges[47] and should not impact photoinduced phase separation. We plot the integrated emission from each channel as a function of time in Figure 1E and see very similar, yet slower, kinetics for cluster formation in the single-crystals as is seen in polycrystalline films (Figure S2). Although we are observing photoinduced phase separation in a single-crystalline nanoplate, we note that the clusters form heterogeneously in both space and time suggesting that photoinduced phase separation is a stochastic nonequilibrium process.

To visualize the transient, stochastic formation of I^--rich clusters in lead halide perovskite nanoplates with higher, subdiffraction limit spatial resolution, and to spatially correlate luminescence with morphology, we employ CL microscopy. We use CL imaging to probe I^--rich cluster formation at the nanoscale by alternating illumination with a 405 nm LED and CL acquisition (Figure 2A). After 10 s of illumination, we observe individual, distinct I^--rich clusters, as shown by the

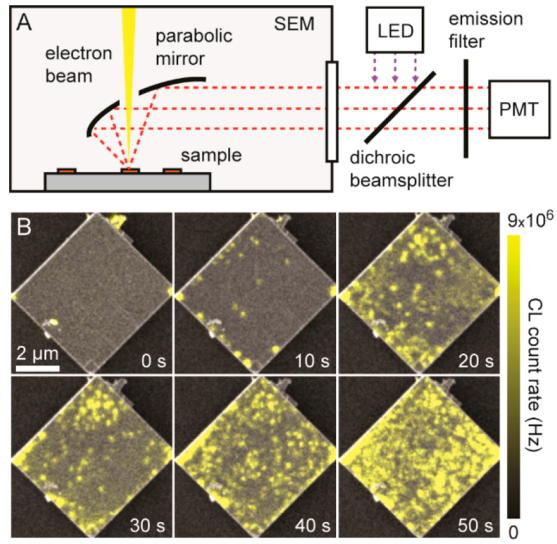

Figure 2. High-resolution cathodoluminescence (CL) imaging of photoinduced phase separation in a single nanoplate. (A) CL detection apparatus. (B) Sequence of CL images with a 650 nm long pass filter interleaved by 10 s of illumination at 405 nm (100 mW/cm^2) between each frame.

bright spots on the CL image superimposed on the secondary electron (SE) image (Figure 2B and Figure S3). For a single nanoplate, we find that I^--rich clusters form in different locations each time we repeat the cycle of inducing phase separation, imaging with CL, and allowing the halide anions to remix (Figure S4). The fact that I^--rich clusters do not repeatedly appear in the same locations indicates that, in single-crystalline nanoplates, the formation of stable I^--rich clusters is not predetermined by spatial variations in static defects. We cannot, however, rule out effects from fluctuations in mobile defects. Local stochastic variations in mobile defect densities, particularly in the form of density fluctuations of halide vacancies, could also impact the formation of I^--rich clusters. Nevertheless, it is expected that inhomogeneities in average defect concentration due to the surface of the plates decay over microscopic length scales given the material's elastic properties.

To further investigate the process of I^--rich cluster formation, we use confocal microscopy at low laser power and find that our observations agree well with simulations. Using low power confocal imaging (~4 μW, 25 mJ/cm^2) to both induce and probe cluster formation, we find that I^--rich clusters form in random locations, appearing as diffraction-limited spots in both nanoplates (Figure 3A and Movie S1) and nanowires (Figure 3B and Movie S2). Although some I^--rich clusters appear momentarily, other clusters are stable over much longer time periods. By performing coarse-grained dynamics simulations of multiple polarons in a mixed halide lattice (Figure 3C and Movie S3), we confirm that charge carriers both stabilize and are trapped in regions of high I^- content. Charge carrier trapping requires an I^- composition fluctuation above a critical size, which is why at short times bright clusters form and dissolve stochastically.

To demonstrate that reducing electron−phonon coupling prevents the formation of a phase-separated steady state, we

DOI: 10.1021/acs.jpclett.8b01512
J. Phys. Chem. Lett. 2018, 9, 3998−4005

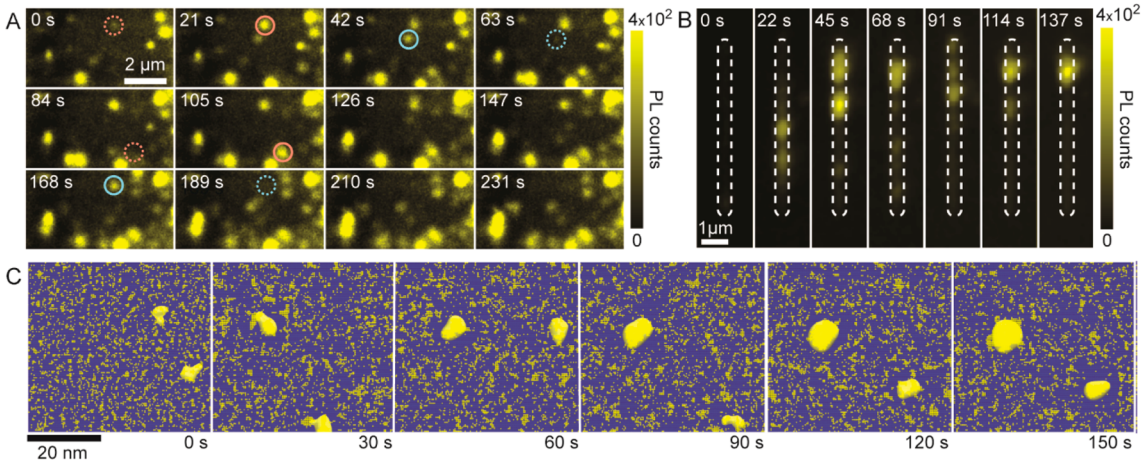

Figure 3. Stochastic formation of iodide-rich domains in $MAPb(I_{0.14}Br_{0.86})_3$ under laser scanning excitation and simulation of cluster formation. (A) Time series of confocal images of the center of a single nanoplate of $MAPb(I_{0.14}Br_{0.86})_3$ taken at low power laser excitation (4 μW with an 8 μs pixel dwell time, or 25 mJ/cm^2), showing blinking of iodide-rich regions within the plate. Red dotted circles indicate the position where a cluster subsequently appears as indicated by a solid red circle. Blue circles indicate where a cluster is about to disappear, while blue dotted circles show the absence of this cluster. (B) Stochastic formation of iodide-rich clusters in a nanowire of the same composition upon confocal laser scanning. (C) Simulation of cluster formation within the perovskite lattice showing the transient appearance of iodide-rich clusters within the plate, as well as longer-lived clusters.

have developed a cation exchange reaction that substitutes Cs^+ for MA^+. A more detailed discussion of the cation exchange, along with associated results (Figure S5 and S6), is found in the Supporting Information, as well as a comparison to other reports of cation exchange in halide perovskites.[48−51] Using this cation exchange, we show that replacing some MA^+ with Cs^+ suppresses phase separation by preventing the polaronic stabilization of I^--rich clusters, but it does not eliminate transient I^- clustering. The cation exchange reaction was performed by submerging nanoplates composed of $MAPb(I_{0.14}Br_{0.86})_3$ in CsI/CsBr in anhydrous isopropyl alcohol (see Supporting Information for further details). Using low-dose TEM SAED, we confirm that the resulting Cs^+/MA^+ alloy nanoplates remain single-crystalline after cation exchange (Figure S7). Using TEM EDS, we show that the resulting nanoplates have a chemical composition of $Cs_{0.39}MA_{0.61}Pb(I_{0.15}Br_{0.85})_3$ after cation exchange to form mixed cation, mixed halide single-crystalline perovskite nanoplates (Figure S8). We compare photoinduced effects in these nanoplates after cation exchange to those that have not undergone cation exchange using the same imaging conditions. At short exposure times (<1 min), we observe formation and disappearance of I^--rich clusters in both mixed cation and pure MA^+ nanoplates (Figure 4A and Movie S4). Nevertheless, at longer exposure times (~3 min), we only observe stable phase separation in the MA^+ nanoplates; the mixed cation nanoplates continue to show transient clustering (Figure 4B and Movie S5). Our results demonstrate that I^--rich clusters exist in the mixed cation perovskites but that the photoinduced charge carriers do not produce substantial enough local strain to stabilize the clusters indefinitely to reach a phase-separated steady state.

Simulations corroborate our imaging results and demonstrate a difference in the extent of polaronic strain in halide perovskites with Cs^+ and MA^+ as the A-site cation. By simulating cluster formation in both Cs^+ and MA^+ mixed halide perovskites using the same coarse-grained framework as in Figure 3C, we can directly compare our simulations of iodide clustering to experiment. The simulation reveals transient cluster formation in both cases, yet I^--rich clusters fail to stabilize for long periods of time in the pure Cs^+ plates, preventing the system from reaching a phase-separated steady state (Movie S6). We find that there is a good match between theory (Figure 4C) and experiment (Figure 4D) in terms of the time scale and extent of cluster stabilization for both types of perovskites. In both cases, phase separation persists in the MA^+ mixed halide perovskite, but it does not with Cs^+ (simulation) or mixed cation (experimental) mixed halide perovskites. Quasiparticle ring polymer molecular dynamics simulations reveal that the Cs^+ mixed halide perovskite exhibits a more weakly bound, larger polaron compared to the MA^+ lattice, with a smaller accompanying strain field and thus a reduced driving force for phase separation. These results are in agreement with expectations from Fröhlich theory.[52] These features are also in agreement with expectations from our previous phenomenological theory, where the reduction in electron−phonon coupling is due to the smaller polarizability of the Cs^+ lattice, which is well described with the empirical force fields employed.[53] Incidentally, we note that differences in the electron−phonon coupling of the two lattices are much more significant than differences in the exciton binding energies at room temperature.[54,55] Snapshots of the molecular dynamics simulations for MA^+ and Cs^+ perovskites are shown in Figure 4E,F, respectively, where the ratio of polaron radii is 0.7. The coarse-grained simulations also show how the distribution of halides at the polaron location changes as a function of illumination time in each case (Figure 4G), with the basic time scale for concentration fluctuations set by the known hopping rate of a halide ion, 1 ms.[56] For the MA^+ mixed halide perovskite, the local distribution of halides shifts drastically toward becoming more I^--rich within 100 s. By contrast, the local distribution of halides in the Cs^+-containing mixed halide perovskite shifts only slightly toward becoming more I^--rich compared to what is expected from random fluctuations in the dark. Additionally, the simulations show that the persistence time of the I^- concentration fluctuations in pure Cs^+-containing perovskites is only slightly greater than that expected due to halide migration in the dark (Movie S6). Mixtures of A cations with intermediate electron−phonon

DOI: 10.1021/acs.jpclett.8b01512
J. Phys. Chem. Lett. 2018, 9, 3998−4005

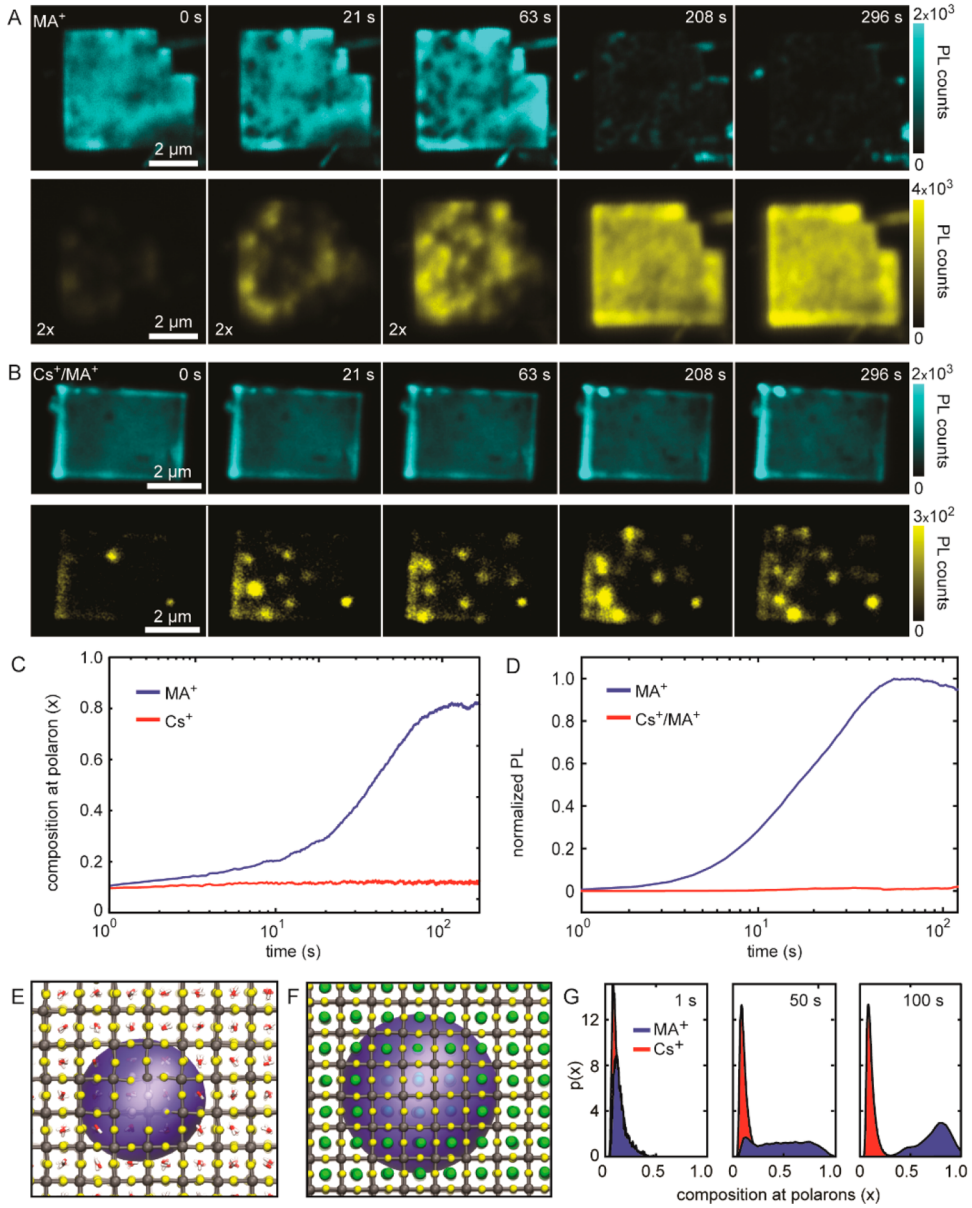

Figure 4. Cation exchange suppresses photoinduced phase separation. Confocal imaging of nanoplates composed of (A) $MAPb(I_{0.14}Br_{0.86})_3$ and (B) $Cs_{0.39}MA_{0.61}Pb(I_{0.15}Br_{0.85})_3$ after cation exchange. The blue channel corresponds to the original emission wavelength (500−560 nm) and the yellow channel corresponds to the I^--rich cluster emission (650−750 nm). The intensity of the first three frames of the yellow channel in B are multiplied by 2x to enhance the contrast at early times. (C) Simulated time trace of the composition at the polaron for $MAPb(I_{0.15}Br_{0.85})_3$ and $CsPb(I_{0.15}Br_{0.85})_3$. (D) PL intensity as a function of time for the PL peak corresponding to iodide-rich regions in the perovskite for $MAPb(I_{0.14}Br_{0.86})_3$ and $Cs_{0.39}MA_{0.65}Pb(I_{0.15}Br_{0.85})_3$. Snapshot of a molecular dynamics (MD) simulation of a polaron 99% isosurface in the $MAPbI_3$ lattice (E) and $CsPbI_3$ lattice (F). (G) Simulated plots of the halide composition at the polaron location at different illumination times using coarse-grained simulations.

coupling strengths, like the one demonstrated experimentally in Figure 4, should therefore have clusters persisting for longer periods of time than for the case of pure Cs^+. Because the presence of transient I^--clusters cannot be fully avoided even by substituting Cs^+ for MA^+, electron−phonon coupling in mixed halide perovskites, regardless of the choice of A site cation, has significant consequences when using these materials in optoelectronic devices.

The combination of nanoscale imaging and molecular modeling of illuminated single-crystal mixed halide perovskites demonstrates that photoinduced phase separation is an inherent process of the perovskite material and not purely a consequence of the microstructure. This has important implications for device applications, as our experiments demonstrate that focusing on improving compositional uniformity by reducing defects, such as reducing the number of grain boundaries, will not suppress photoinduced phase separation in mixed halide hybrid perovskites. Instead, a viable strategy for suppressing phase separation is to reduce electron−phonon coupling. We suggest that postsynthetic treatments that substitute cations and lead to less polar lattices will suppress phase separation, serving as a viable strategy to mitigate photoinduced phase separation in mixed halide perovskites. For example, one could fabricate a film that is susceptible to photoinduced phase separation, such as $MAPb(I_xBr_{1-x})_3$, and then perform a postsynthetic cation

DOI: 10.1021/acs.jpclett.8b01512
J. Phys. Chem. Lett. 2018, 9, 3998−4005

exchange, converting the film to $Cs_yMa_{1-y}Pb(I_xBr_{1-x})_3$, to lower the electron−phonon coupling, preventing photoinduced effects while preserving the more favorable morphology of the MA-based film. While this prescription represents an important advance, it is important to remain aware of the fact that even though a phase-separated steady state is prevented when Cs^+ is introduced into the lattice, transient I^- clustering could still decrease device performance, albeit by a lesser amount. For instance, we find that the photoluminescence of the mixed cation perovskite nanoplates dropped by approximately 10% upon illumination because of transient I^--rich cluster formation. This decrease in photoluminescence quantum yield should correlate to a decrease in the photovoltage of a solar cell made from this material.[54]

Even though structural defects are not directly responsible for photoinduced phase separation, they do play a supporting role. The presence of vacancies is directly responsible for the mobility of halides in the lattice, changing the kinetics of photoinduced phase separation. In addition, the relationship between lattice strain and clustering dynamics requires deeper investigation. Inherent strain in the perovskite lattice resulting from rapid crystallization during solution processing could significantly affect electron−phonon coupling and the propensity of the halides to phase separate under illumination. Furthermore, the relationship between defect density and electron−photon coupling in these materials is also not well understood. Both variations in defect concentrations and lattice strain could explain inconsistencies in observations of photoinduced phase separation in mixed cation, mixed halide perovskites.[13,19] Nevertheless, we have provided a body of evidence that photoinduced phase separation results from intrinsic properties of mixed halide perovskites. Furthermore, although it can be significantly suppressed by strategically altering the interactions between charge carriers and the perovskite lattice, we have also shown how the transient halide demixing that occurs even when these interactions are minimized may continue to limit the efficiency of optoelectronic devices based on mixed halide perovskites.

■ ASSOCIATED CONTENT

Supporting Information

The Supporting Information is available free of charge on the ACS Publications website at DOI: 10.1021/acs.jpclett.8b01512.

Experimental materials and methods, simulation methods, a further discussion of the cation exchange, energy dispersive X-ray spectroscopy of the plates, comparison in the kinetics of photoinduced phase separation in thin films versus plates, additional CL images of single crystal plates, and XRD and EDS post cation exchange (PDF)

Movie S1: Blinking in mixed halide nanoplate (AVI)

Movie S2: Blinking in mixed halide nanowire (AVI)

Movie S3: Coarse-grained simulation of photoinduced phase separation in a MA^+ mixed halide perovskite (AVI)

Movie S4: Confocal imaging movie showing photoinduced phase separation in a MA^+ mixed halide perovskite nanoplate ($MAPb(I_{0.14}Br_{0.86})_3$) (AVI)

Movie S5: Confocal imaging movie showing transient iodide clustering in a Cs^+ mixed halide perovskite nanoplates ($Cs_{0.39}MA_{0.61}Pb(I_{0.15}Br_{0.85})_3$) (AVI)

Movie S6: Coarse-grained simulation of photoinduced phase separation in a Cs^+ mixed halide perovskite (AVI)

■ AUTHOR INFORMATION

Corresponding Author

*E-mail: nsginsberg@berkeley.edu.

ORCID

Connor G. Bischak: 0000-0002-3071-4069
Andrew B. Wong: 0000-0002-0731-1931
Peidong Yang: 0000-0003-4799-1684
Naomi S. Ginsberg: 0000-0002-5660-3586

Present Addresses

▽Department of Chemistry, University of Washington, Seattle, WA, 98195, United States
○Department of Chemical Engineering, Stanford University, Stanford, CA 94305, United States
◆Department of Computer Science, Stanford University, Stanford, CA 94305, United States

Author Contributions

¶These authors contributed equally to this work

Notes

The authors declare no competing financial interest.

■ ACKNOWLEDGMENTS

The portion of this work on the development and characterization of cation exchange reactions was funded by the U.S. Department of Energy, Office of Science, Office of Basic Energy Sciences, Materials Sciences and Engineering Division under Contract No. DE-AC02-05-CH11231 within the Physical Chemistry of Inorganic Nanostructures Program (KC3103). The CL imaging at the Lawrence Berkeley Lab Molecular Foundry and the TEM imaging at the National Center for Electron Microscopy were performed as part of the Molecular Foundry user program, supported by the Office of Science, Office of Basic Energy Sciences, of the U.S. Department of Energy under Contract No. DE-AC02-05CH11231. PL and CL imaging were supported by a David and Lucile Packard Fellowship for Science and Engineering awarded to N.S.G. and by STROBE, A National Science Foundation Science and Technology Center under Grant No. DMR 1548924. A.B.W. acknowledges support from the Lam Research Graduate Fellowship. C.G.B. acknowledges an NSF Graduate Research Fellowship (DGE 1106400), and N.S.G. acknowledges an Alfred P. Sloan Research Fellowship and a Camille Dreyfus Teacher-Scholar Award. D.T.L. was supported by the UC Berkeley College of Chemistry.

■ REFERENCES

(1) Leguy, A. M. A.; Frost, J. M.; McMahon, A. P.; Sakai, V. G.; Kockelmann, W.; Law, C.; Li, X.; Foglia, F.; Walsh, A.; O'Regan, B. C.; et al. The Dynamics of Methylammonium Ions in Hybrid Organic-Inorganic Perovskite Solar Cells. *Nat. Commun.* **2015**, *6*, 7124.

(2) Mattoni, A.; Filippetti, A.; Saba, M. I.; Delugas, P. Methylammonium Rotational Dynamics in Lead Halide Perovskite by Classical Molecular Dynamics: The Role of Temperature. *J. Phys. Chem. C* **2015**, *119* (30), 17421−17428.

(3) Hoke, E. T.; Slotcavage, D. J.; Dohner, E. R.; Bowring, A. R.; Karunadasa, H. I.; McGehee, M. D. Reversible Photo-Induced Trap Formation in Mixed-Halide Hybrid Perovskites for Photovoltaics. *Chem. Sci.* **2015**, *6* (1), 613−617.

DOI: 10.1021/acs.jpclett.8b01512
J. Phys. Chem. Lett. 2018, 9, 3998−4005

(4) deQuilettes, D. W.; Zhang, W.; Burlakov, V. M.; Graham, D. J.; Leijtens, T.; Osherov, A.; Bulović, V.; Snaith, H. J.; Ginger, D. S.; Stranks, S. D. Photo-Induced Halide Redistribution in Organic-Inorganic Perovskite Films. *Nat. Commun.* **2016**, *7*, 11683.
(5) Stranks, S. D.; Eperon, G. E.; Grancini, G.; Menelaou, C.; Alcocer, M. J. P.; Leijtens, T.; Herz, L. M.; Petrozza, A.; Snaith, H. J. Electron-Hole Diffusion Lengths Exceeding 1 Micrometer in an Organometal Trihalide Perovskite Absorber. *Science* **2013**, *342* (6156), 341−344.
(6) deQuilettes, D. W.; Vorpahl, S. M.; Stranks, S. D.; Nagaoka, H.; Eperon, G. E.; Ziffer, M. E.; Snaith, H. J.; Ginger, D. S. Impact of Microstructure on Local Carrier Lifetime in Perovskite Solar Cells. *Science* **2015**, *348*, 683−686.
(7) Dong, Q.; Fang, Y.; Shao, Y.; Mulligan, P.; Qiu, J.; Cao, L.; Huang, J. Electron-Hole Diffusion Lengths > 175 μm in Solution-Grown $CH_3NH_3PbI_3$ Single Crystals. *Science* **2015**, *347* (6225), 967−970.
(8) Tan, Z.-K.; Moghaddam, R. S.; Lai, M. L.; Docampo, P.; Higler, R.; Deschler, F.; Price, M.; Sadhanala, A.; Pazos, L. M.; Credgington, D.; et al. Bright Light-Emitting Diodes Based on Organometal Halide Perovskite. *Nat. Nanotechnol.* **2014**, *9* (9), 687−692.
(9) Wong, A. B.; Lai, M.; Eaton, S. W.; Yu, Y.; Lin, E.; Dou, L.; Fu, A.; Yang, P. Growth and Anion Exchange Conversion of $CH_3NH_3PbX_3$ Nanorod Arrays for Light-Emitting Diodes. *Nano Lett.* **2015**, *15* (8), 5519−5524.
(10) Zhu, H.; Fu, Y.; Meng, F.; Wu, X.; Gong, Z.; Ding, Q.; Gustafsson, M. V.; Trinh, M. T.; Jin, S.; Zhu, X.-Y. Lead Halide Perovskite Nanowire Lasers with Low Lasing Thresholds and High Quality Factors. *Nat. Mater.* **2015**, *14* (6), 636−642.
(11) Eaton, S. W.; Lai, M.; Gibson, N. A.; Wong, A. B.; Dou, L.; Ma, J.; Wang, L.-W.; Leone, S. R.; Yang, P. Lasing in Robust Cesium Lead Halide Perovskite Nanowires. *Proc. Natl. Acad. Sci. U. S. A.* **2016**, *113* (8), 1993−1998.
(12) Bailie, C. D.; Christoforo, M. G.; Mailoa, J. P.; Bowring, A. R.; Unger, E. L.; Nguyen, W. H.; Burschka, J.; Pellet, N.; Lee, J. Z.; Grätzel, M.; et al. Semi-Transparent Perovskite Solar Cells for Tandems with Silicon and CIGS. *Energy Environ. Sci.* **2015**, *8* (3), 956−963.
(13) McMeekin, D. P.; Sadoughi, G.; Rehman, W.; Eperon, G. E.; Saliba, M.; Hörantner, M. T.; Haghighirad, A.; Sakai, N.; Korte, L.; Rech, B.; et al. A Mixed-Cation Lead Mixed-Halide Perovskite Absorber for Tandem Solar Cells. *Science* **2016**, *351* (6269), 151−155.
(14) Eperon, G. E.; Leijtens, T.; Bush, K. A.; Prasanna, R.; Green, T.; Wang, J. T.-W.; McMeekin, D. P.; Volonakis, G.; Milot, R. L.; May, R.; et al. Perovskite-Perovskite Tandem Photovoltaics with Optimized Bandgaps. *Science* **2016**, *354*, 861−865.
(15) Noh, J. H.; Im, S. H.; Heo, J. H.; Mandal, T. N.; Seok, S. I. Chemical Management for Colorful, Efficient, and Stable Inorganic−Organic Hybrid Nanostructured Solar Cells. *Nano Lett.* **2013**, *13* (4), 1764−1769.
(16) Sadhanala, A.; Deschler, F.; Thomas, T. H.; Dutton, S. E.; Goedel, K. C.; Hanusch, F. C.; Lai, M. L.; Steiner, U.; Bein, T.; Docampo, P.; et al. Preparation of Single-Phase Films of $CH_3NH_3Pb(I_{1-x}Br_x)_3$ with Sharp Optical Band Edges. *J. Phys. Chem. Lett.* **2014**, *5* (15), 2501−2505.
(17) Xiao, J.-W.; Liu, L.; Zhang, D.; De Marco, N.; Lee, J.-W.; Lin, O.; Chen, Q.; Yang, Y. The Emergence of the Mixed Perovskites and Their Applications as Solar Cells. *Adv. Energy Mater.* **2017**, *7* (20), 1700491.
(18) Yoon, S. J.; Draguta, S.; Manser, J. S.; Sharia, O.; Schneider, W. F.; Kuno, M.; Kamat, P. V. Tracking Iodide and Bromide Ion Segregation in Mixed Halide Lead Perovskites during Photo-irradiation. *ACS Energy Lett.* **2016**, *1* (1), 290−296.
(19) Beal, R. E.; Slotcavage, D. J.; Leijtens, T.; Bowring, A. R.; Belisle, R. A.; Nguyen, W. H.; Burkhard, G. F.; Hoke, E. T.; McGehee, M. D. Cesium Lead Halide Perovskites with Improved Stability for Tandem Solar Cells. *J. Phys. Chem. Lett.* **2016**, *7* (5), 746−751.
(20) Slotcavage, D. J.; Karunadasa, H. I.; McGehee, M. D. Light-Induced Phase Segregation in Halide-Perovskite Absorbers. *ACS Energy Lett.* **2016**, *1* (6), 1199−1205.
(21) Bischak, C. G.; Hetherington, C. L.; Wu, H.; Aloni, S.; Ogletree, D. F.; Limmer, D. T.; Ginsberg, N. S. Origin of Reversible Photoinduced Phase Separation in Hybrid Perovskites. *Nano Lett.* **2017**, *17* (2), 1028−1033.
(22) Barker, A. J.; Sadhanala, A.; Deschler, F.; Gandini, M.; Senanayak, S. P.; Pearce, P. M.; Mosconi, E.; Pearson, A. J.; Wu, Y.; Srimath Kandada, A. R.; et al. Defect-Assisted Photoinduced Halide Segregation in Mixed-Halide Perovskite Thin Films. *ACS Energy Lett.* **2017**, *2* (6), 1416−1424.
(23) Li, Y.; El Gabaly, F.; Ferguson, T. R.; Smith, R. B.; Bartelt, N. C.; Sugar, J. D.; Fenton, K. R.; Cogswell, D. A.; Kilcoyne, A. L. D.; Tyliszczak, T.; et al. Current-Induced Transition from Particle-by-Particle to Concurrent Intercalation in Phase-Separating Battery Electrodes. *Nat. Mater.* **2014**, *13* (12), 1149−1156.
(24) Draguta, S.; Sharia, O.; Yoon, S. J.; Brennan, M. C.; Morozov, Y. V.; Manser, J. M.; Kamat, P. V.; Schneider, W. F.; Kuno, M. Rationalizing the Light-Induced Phase Separation of Mixed Halide Organic−inorganic Perovskites. *Nat. Commun.* **2017**, *8* (1), 200.
(25) Yoon, S. J.; Kuno, M.; Kamat, P. V. Shift Happens. How Halide Ion Defects Influence Photoinduced Segregation in Mixed Halide Perovskites. *ACS Energy Lett.* **2017**, *2* (7), 1507−1514.
(26) Lang, F.; Shargaieva, O.; Brus, V. V.; Neitzert, H. C.; Rappich, J.; Nickel, N. H. Influence of Radiation on the Properties and the Stability of Hybrid Perovskites. *Adv. Mater.* **2018**, *30*, 1702905.
(27) Samu, G. F.; Janáky, C.; Kamat, P. V. A Victim of Halide Ion Segregation. How Light Soaking Affects Solar Cell Performance of Mixed Halide Lead Perovskites. *ACS Energy Lett.* **2017**, *2* (8), 1860−1861.
(28) Braly, I. L.; Stoddard, R. J.; Rajagopal, A.; Uhl, A. R.; Katahara, J. K.; Jen, A. K.-Y.; Hillhouse, H. W. Current-Induced Phase Segregation in Mixed Halide Hybrid Perovskites and Its Impact on Two-Terminal Tandem Solar Cell Design. *ACS Energy Lett.* **2017**, *2* (8), 1841−1847.
(29) Xiao, Z.; Zhao, L.; Tran, N. L.; Lin, Y. L.; Silver, S. H.; Kerner, R. A.; Yao, N.; Kahn, A.; Scholes, G. D.; Rand, B. P. Mixed-Halide Perovskites with Stabilized Bandgaps. *Nano Lett.* **2017**, *17* (11), 6863−6869.
(30) Tang, X.; van den Berg, M.; Gu, E.; Horneber, A.; Matt, G. J.; Osvet, A.; Meixner, A. J.; Zhang, D.; Brabec, C. J. Local Observation of Phase Segregation in Mixed-Halide Perovskite. *Nano Lett.* **2018**, *18* (3), 2172−2178.
(31) Sutter-Fella, C. M.; Ngo, Q. P.; Cefarin, N.; Gardner, K.; Tamura, N.; Stan, C. V.; Drisdell, W. S.; Javey, A.; Toma, F. M.; Sharp, I. D. Cation-Dependent Light-Induced Halide Demixing in Hybrid Organic-Inorganic Perovskites. *Nano Lett.* **2018**, *18* (6), 3473−3480.
(32) Cappel, U. B.; Svanström, S.; Lanzilotto, V.; Johansson, F. O. L.; Aitola, K.; Philippe, B.; Giangrisostomi, E.; Ovsyannikov, R.; Leitner, T.; Föhlisch, A.; et al. Partially Reversible Photoinduced Chemical Changes in a Mixed-Ion Perovskite Material for Solar Cells. *ACS Appl. Mater. Interfaces* **2017**, *9* (40), 34970−34978.
(33) Bischak, C. G.; Sanehira, E. M.; Precht, J. T.; Luther, J. M.; Ginsberg, N. S. Heterogeneous Charge Carrier Dynamics in Organic−Inorganic Hybrid Materials: Nanoscale Lateral and Depth-Dependent Variation of Recombination Rates in Methylammonium Lead Halide Perovskite Thin Films. *Nano Lett.* **2015**, *15* (7), 4799−4807.
(34) Dou, L.; Wong, A. B.; Yu, Y.; Lai, M.; Kornienko, N.; Eaton, S. W.; Fu, A.; Bischak, C. G.; Ma, J.; Ding, T.; et al. Atomically Thin Two-Dimensional Organic-Inorganic Hybrid Perovskites. *Science* **2015**, *349* (6255), 1518−1521.
(35) Xiao, C.; Li, Z.; Guthrey, H.; Moseley, J.; Yang, Y.; Wozny, S.; Moutinho, H.; To, B.; Berry, J. J.; Gorman, B.; et al. Mechanisms of Electron-Beam-Induced Damage in Perovskite Thin Films Revealed by Cathodoluminescence Spectroscopy. *J. Phys. Chem. C* **2015**, *119* (48), 26904−26911.

DOI: 10.1021/acs.jpclett.8b01512
J. Phys. Chem. Lett. 2018, 9, 3998−4005

(36) Hentz, O.; Zhao, Z.; Gradečak, S. Impacts of Ion Segregation on Local Optical Properties in Mixed Halide Perovskite Films. *Nano Lett.* **2016**, *16* (2), 1485−1490.
(37) Dar, M. I.; Hinderhofer, A.; Jacopin, G.; Belova, V.; Arora, N.; Zakeeruddin, S. M.; Schreiber, F.; Grätzel, M. Function Follows Form: Correlation between the Growth and Local Emission of Perovskite Structures and the Performance of Solar Cells. *Adv. Funct. Mater.* **2017**, *27* (26), 1701433.
(38) Lai, M.; Kong, Q.; Bischak, C. G.; Yu, Y.; Dou, L.; Eaton, S. W.; Ginsberg, N. S.; Yang, P. Structural, Optical, and Electrical Properties of Phase-Controlled Cesium Lead Iodide Nanowires. *Nano Res.* **2017**, *10*, 1107−1114.
(39) Onoda-Yamamuro, N.; Matsuo, T.; Suga, H. Dielectric Study of $CH_3NH_3PbX_3$ (X = Cl, Br, I). *J. Phys. Chem. Solids* **1992**, *53* (7), 935−939.
(40) Johnston, M. B.; Herz, L. M. Hybrid Perovskites for Photovoltaics: Charge-Carrier Recombination, Diffusion, and Radiative Efficiencies. *Acc. Chem. Res.* **2016**, *49* (1), 146−154.
(41) Galkowski, K.; Mitioglu, A.; Miyata, A.; Plochocka, P.; Portugall, O.; Eperon, G. E.; Wang, J. T.-W.; Stergiopoulos, T.; Stranks, S. D.; Snaith, H. J.; et al. Determination of the Exciton Binding Energy and Effective Masses for Methylammonium and Formamidinium Lead Tri-Halide Perovskite Semiconductors. *Energy Environ. Sci.* **2016**, *9* (3), 962−970.
(42) Zhu, H.; Miyata, K.; Fu, Y.; Wang, J.; Joshi, P. P.; Niesner, D.; Williams, K. W.; Jin, S.; Zhu, X.-Y. Screening in Crystalline Liquids Protects Energetic Carriers in Hybrid Perovskites. *Science* **2016**, *353* (6306), 1409−1413.
(43) Miyata, K.; Meggiolaro, D.; Trinh, M. T.; Joshi, P. P.; Mosconi, E.; Jones, S. C.; De Angelis, F.; Zhu, X.-Y. Large Polarons in Lead Halide Perovskites. *Sci. Adv.* **2017**, *3* (8), e1701217.
(44) Ivanovska, T.; Dionigi, C.; Mosconi, E.; De Angelis, F.; Liscio, F.; Morandi, V.; Ruani, G. Long-Lived Photoinduced Polarons in Organohalide Perovskites. *J. Phys. Chem. Lett.* **2017**, *8* (13), 3081−3086.
(45) Guzelturk, B.; Belisle, R. A.; Smith, M. D.; Bruening, K.; Prasanna, R.; Yuan, Y.; Gopalan, V.; Tassone, C. J.; Karunadasa, H. I.; McGehee, M. D.; et al. Terahertz Emission from Hybrid Perovskites Driven by Ultrafast Charge Separation and Strong Electron−Phonon Coupling. *Adv. Mater.* **2018**, *30* (11), 1704737.
(46) Zhang, Q.; Su, R.; Liu, X.; Xing, J.; Sum, T. C.; Xiong, Q. High-Quality Whispering-Gallery-Mode Lasing from Cesium Lead Halide Perovskite Nanoplatelets. *Adv. Funct. Mater.* **2016**, *26* (34), 6238−6245.
(47) Dar, M. I.; Jacopin, G.; Hezam, M.; Arora, N.; Zakeeruddin, S. M.; Deveaud, B.; Nazeeruddin, M. K.; Grätzel, M. Asymmetric Cathodoluminescence Emission in $CH_3NH_3PbI_{3-x}Br_x$ Perovskite Single Crystals. *ACS Photonics* **2016**, *3* (6), 947−952.
(48) Eperon, G. E.; Beck, C. E.; Snaith, H. J. Cation Exchange for Thin Film Lead Iodide Perovskite Interconversion. *Mater. Horiz.* **2016**, *3* (1), 63−71.
(49) Niemann, R. G.; Gouda, L.; Hu, J.; Tirosh, S.; Gottesman, R.; Cameron, P. J.; Zaban, A. Cs^+ Incorporation into $CH_3NH_3PbI_3$ Perovskite: Substitution Limit and Stability Enhancement. *J. Mater. Chem. A* **2016**, *4* (45), 17819−17827.
(50) van der Stam, W.; Geuchies, J. J.; Altantzis, T.; van den Bos, K. H. W.; Meeldijk, J. D.; Van Aert, S.; Bals, S.; Vanmaekelbergh, D.; de Mello Donega, C. Highly Emissive Divalent-Ion-Doped Colloidal $CsPb_{1-x}M_xBr_3$ Perovskite Nanocrystals through Cation Exchange. *J. Am. Chem. Soc.* **2017**, *139* (11), 4087−4097.
(51) Eperon, G. E.; Ginger, D. S. B-Site Metal Cation Exchange in Halide Perovskites. *ACS Energy Lett.* **2017**, *2* (5), 1190−1196.
(52) Frost, J. M. Calculating Polaron Mobility in Halide Perovskites. *Phys. Rev. B: Condens. Matter Mater. Phys.* **2017**, *96* (19), 195202.
(53) Mattoni, A.; Filippetti, A.; Caddeo, C. Modeling Hybrid Perovskites by Molecular Dynamics. *J. Phys.: Condens. Matter* **2017**, *29* (4), 043001.
(54) Zheng, K.; Zhu, Q.; Abdellah, M.; Messing, M. E.; Zhang, W.; Generalov, A.; Niu, Y.; Ribaud, L.; Canton, S. E.; Pullerits, T. Exciton Binding Energy and the Nature of Emissive States in Organometal Halide Perovskites. *J. Phys. Chem. Lett.* **2015**, *6* (15), 2969−2975.
(55) Yang, Z.; Surrente, A.; Galkowski, K.; Miyata, A.; Portugall, O.; Sutton, R. J.; Haghighirad, A. A.; Snaith, H. J.; Maude, D. K.; Plochocka, P.; et al. Impact of the Halide Cage on the Electronic Properties of Fully Inorganic Cesium Lead Halide Perovskites. *ACS Energy Lett.* **2017**, *2* (7), 1621−1627.
(56) Eames, C.; Frost, J. M.; Barnes, P. R. F.; O'Regan, B. C.; Walsh, A.; Islam, M. S. Ionic Transport in Hybrid Lead Iodide Perovskite Solar Cells. *Nat. Commun.* **2015**, *6*, 7497.

DOI: 10.1021/acs.jpclett.8b01512
J. Phys. Chem. Lett. 2018, 9, 3998−4005